JOURNAL OF Applied Polymer SCIENCE

Low Percolation Threshold in Polycarbonate/Multiwalled Carbon Nanotubes Nanocomposites Through Melt Blending with Poly(butylene terephthalate)

Sandip Maiti, Supratim Suin, Nilesh K. Shrivastava, B. B. Khatua
Materials Science Centre, Indian Institute of Technology, Kharagpur 721302, India
Correspondence to: B. B. Khatua (E-mail: khatuabb@matsc.iitkgp.ernet.in)

ABSTRACT: Here, we demonstrate an easy method for the preparation of highly electrically conductive polycarbonate (PC)/multiwalled carbon nanotubes (MWCNTs) nanocomposites in the presence of poly(butylene terephthalate) (PBT). In the presence of MWCNTs, PC and PBT formed a miscible blend, and the MWCNTs in the PC matrix were uniformly and homogeneously dispersed after the melt mixing of the PC and PBT–MWCNT mixture. Finally, when the proportion of the PC and PBT–MWCNT mixture in the blend/MWCNT nanocomposites was changed, an electrical conductivity of 6.87×10^{-7} S/cm was obtained in the PC/PBT–MWCNT nanocomposites at an MWCNT loading as low as about 0.35 wt %. Transmission electron microscopy revealed a regular and homogeneous dispersion and distribution of the MWCNTs and formed a continuous conductive network pathway of MWCNTs throughout the matrix phase. The storage modulus and thermal stability of the PC were also enhanced by the presence of a small amount of MWCNTs in the nanocomposites. © 2013 Wiley Periodicals, Inc. J. Appl. Polym. Sci. 130: 543–553, 2013

KEYWORDS: blends; morphology; polycarbonates

Received 20 November 2012; accepted 10 February 2013; published online 20 March 2013
DOI: 10.1002/app.39168

INTRODUCTION

In the last few years, conductive polymer nanocomposites based on conductive particles or nanofillers, such as graphite, carbon black (CB), carbon nanofiber, single/multiwalled carbon nanotubes (MWCNTs), and graphene, incorporated into an insulating polymer matrix have been achieved greater attention because of their broad applications in various fields, including electronics, thermal interface materials, biomedical devices, automotive materials, electromagnetic shielding, and aerospace antistatic and electrically conductive materials.[1,2] Among these nanofillers, carbon nanotubes (CNTs) have been efficiently used in multiple fields, such as sensors,[3] transistors,[4] devices,[5] catalysts,[6] bioluminescent probes,[7] and high-performance[8] nanocomposites because of their unique and extraordinary electrical and mechanical properties. The nanosize, high surface area, and high electrical conductivity of the high aspect ratio (length to diameter) of CNTs offer great opportunities for enhancing the electrical conductivity and thermal and mechanical properties of polymer nanocomposites at a very low CNT loading. The electrical conductivity of the polymer nanocomposites strongly depend on the extent of dispersion and distribution of the nanofillers and its loading in the matrix polymer. In polymer/filler conductive nanocomposites, nanofillers form a continuous conductive network path in the polymer matrix above a critical concentration of the nanofillers, known as the *percolation threshold* (p_c); this is directly proportional to the aspect ratio of the nanofillers and the dispersion of the nanofillers in the polymer matrix.

Several methods, including (1) solution blending of the polymer in the presence of CNTs, (2) *in situ* polymerization of a monomer in the presence of CNTs, and (3) melt blending of the polymer with CNTs, have already been employed for the preparation of polymer/CNT nanocomposites. However, the development of electrical conductivity at a very low CNT loading in most polymer/CNT nanocomposites has been limited by the insufficient dispersion and individualization of the CNTs in polymer matrix.

Polycarbonate (PC) provides a high impact resistance, toughness, dimensional stability, and good optical clarity and is broadly used in several engineering applications. The main disadvantages of PC are its poor chemical resistance and low resistance to abrasion. Thus, PC has been modified in different ways, particularly by blending with different polymers for various demanding applications.[9] Recently, many researchers have modified PC by compounding with CNTs to improve its electrical, mechanical, and thermal properties.[10–22] For instance,

Wu et al.[10] showed that the electrical conductivity of melt-blended PC/functionalized MWCNT nanocomposites was 2×10^{-8} S/cm at a 2 wt % loading of functionalized MWCNTs. King et al.[11] reported that p_c of CNTs in melt-blended PC/-MWCNT nanocomposites was nearly at a 1.4 vol % loading of MWCNTs and achieved an 18 Ω cm electrical resistivity of the nanocomposites at a 4.2 vol % loading of MWCNTs. Hornbostel et al.[12] reported that the p_c of melt-extruded PC/MWCNT nanocomposites appeared between a 1.5 and 2.0 wt % loading of MWCNTs. Lee et al.[13] showed the electrical p_c of solution-blended PC/MWCNT nanocomposites at a 0.91 vol % loading of MWCNTs. Chen et al.[14] studied the electrical conductivity of PC/MWCNT nanocomposites and reported a conductivity value of 1.8×10^{-6} S/cm at a 5 wt % loading of MWCNTs, which was the p_c of the nanocomposites. Yamaguchi et al.[15] reported that the electrical percolation of melt-blended PC/MWCNT nanocomposites prepared by the melt dilution of a PC/MWCNT (20 wt %) mixture was found at about a 3 wt % loading of MWCNTs. Kim and Jo[16] reported that PC/MWCNT nanocomposites exhibited its electrical properties when they were prepared with more than a 1 wt % loading of MWCNTs. Abbasi et al.[17] concluded that the p_c of melt-blended PC/MWCNT nanocomposites prepared by the melt dilution of the PC/MWCNT (15 wt %) mixture with the PC matrix was between 2 and 3 wt % MWCNT loadings. Potschke and coworkers[18,19] reported that the p_c of melt-blended PC/MWCNT nanocomposites prepared by the dilution of a PC/MWCNT (15 wt %) mixture was between 1 and 1.5 wt % MWCNT loadings. Sathpathy et al.[20] studied the electrical conductivity of melt-blended PC/MWCNT nanocomposites and found an electrical conductivity of 2×10^{-8} S/cm at a 2 wt % loading of MWCNTs. Kim et al.[21] studied the electrical conductivity of solution-blended PC/MWCNT nanocomposites and did not find any electrical conductivity, even at a 3 wt % MWCNT loading in the nanocomposites. However, they reported that an electrical p_c of melt-blended PC/MWCNT nanocomposites at high CNT loadings between 1.5 and 2.5 wt %.[22]

Regardless of the methods reported for nanocomposites preparation, the p_c of CNT in the PC matrix was above a 1.0 wt % CNT loading in most of the nanocomposites. This offers a space for developing electrically conducting PC/MWCNT nanocomposites at very low CNT loadings. In this article, we demonstrate a simple and easy method that involves the melt blending of PC and poly(butylene terephthalate) (PBT)–MWCNT mixture for the preparation of PC/MWCNT nanocomposites. The immiscible blend of PC and PBT is well known as *xenoy*,[23] where the PC contributes to good mechanical and thermal properties, and PBT provides chemical resistance, a higher flow, and thermal stability. However, in the presence of MWCNTs in the PBT phases, they were found to form a miscible polymer blend. Here, MWCNTs act as a viscosity modifier and increased the melt viscosity of the PBT phase. When polymer nanocomposites were prepared with nanofiller (MWCNTs), the melt viscosity of the matrix polymer increased, as reported earlier.[24,25] In this study, the melt viscosity of PBT was expected to increase when it was melt-blended with MWCNT, and thus, the melt viscosity of the PBT–MWCNT masterbatch closely approached the melt viscosity value of PC. This minimized the difference between the melt viscosities of these two polymers and helped in the formation of a miscible blend.

In contrast to our previous study on a PS/ABS–MWCNT system,[26] here, we applied a similar method to lower the percolation in the PC matrix by considering the immiscible blend of PC and PBT. Here, the selective dispersion of CNTs in the PBT phase, before the blending of PC/PBT, resulted in miscible PC/PBT/MWCNT nanocomposites. Thus, well-dispersed CNTs in the PBT–MWCNT masterbatch (due to the low viscosity of PBT than PC) finally resulted in the homogeneous dispersion and distribution of the CNTs throughout the PC/PBT miscible matrix; this was similar to the dispersion of CNTs in the matrix of melt-blended PC/MWCNT nanocomposites. Thus, the morphology of the PS/ABS–MWCNT and PC/PBT–MWCNT nanocomposites was entirely different, and the ability of the network structures of CNTs to develop electrical conductivity were also not similar. Thus, the melt blending of PC with the PBT–MWCNT mixture may have resulted in a homogeneous dispersion and distribution of the CNTs in the PC matrix and led to the development of electrical conductivity at very low CNT loadings.

EXPERIMENTAL

Materials Details

General purpose, transparent PC (Lexan 143; density = 1.19 g/cc, melt flow index = 10.5 g/10 min at 300°C and 1.2 kg load) pellets (average diameter ≈ 2.75 mm, length ≈ 3.35 mm), and semicrystalline PBT (Valox resin 175; density = 1.32 g/cc, melt flow index = 127 g/10 min at 250°C and 1.2 kg load) pellets (average diameter ≈2.75 mm, length ≈3.75 mm) were obtained from SABIC Innovative Plastics (formerly General Electric Plastics), Netherlands. The MWCNTs employed in this study were industrial grade (NC 7000 series; average diameter = 9.5 nm, length = 1.5 μm, surface area = 250–300 m^2/g, 90% carbon purity) and were purchased from Nanocyl S.A. (Sambreville, Belgium). The MWCNTs were used as received without any further chemical modification.

Preparation of the Composites

In this study, miscible PC/PBT–MWCNT nanocomposites with various MWCNT loadings were prepared by the melt blending of a PBT–MWCNT mixture (prepared by the melt mixing of PBT and MWCNTs) with different ratios of PC. First, the pure PC, pure PBT, and MWCNTs were dried in a vacuum oven at about 80°C for 12 h to remove the moisture.[25,27] Then, a masterbatch of PBT and MWCNTs with a 3.5 wt % loading of MWCNTs was prepared with an internal mixer (Brabender Plasticorder, with a chamber capacity of 20 cc) at 240°C and 60 rpm for 12 min. The PBT–MWCNT masterbatch was then melt-mixed with pure PC at different compositions at 280°C and 60 rpm for 15 min. A schematic representation for the preparation of the PC/PBT–MWCNT nanocomposites is shown in Figure 1. The figure shows that the PC/PBT blend was immiscible in nature. However, it was shown that PC and PBT were miscible in the PC/PBT–MWCNT nanocomposites. Here, MWCNTs acted as a viscosity modifier; this increased the melt viscosity of PBT and, thus, resulted in proper matching

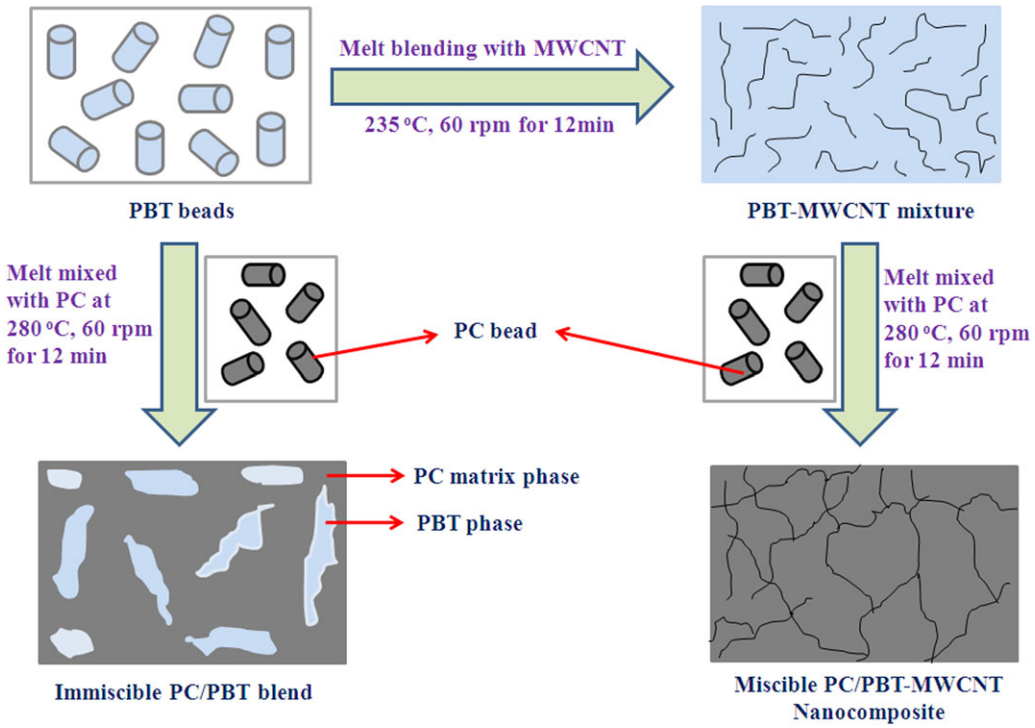

Figure 1. Schematic representation for the preparation of the PC/PBT–MWCNT nanocomposites. [Color figure can be viewed in the online issue, which is available at wileyonlinelibrary.com.]

in the melt viscosities of the two polymers to form miscible blend/MWCNT nanocomposites. With the addition of MWCNTs, an interconnected or networklike structure was formed throughout the matrix polymer because of the entanglement of the polymer chains with the tubelike, high-aspect-ratio MWCNTs and resulted in filler–filler or filler–polymer interactions. Thus, nanocomposites were observed to exhibit shear-thinning behavior. This behavior increased with increasing nanofiller loading in the nanocomposites; this helped to increase the melt viscosity of the nanocomposites with the incorporation of MWCNTs. Thus, the melt viscosity value of PBT in the PBT/MWCNT phase approached the melt viscosity of the PC and resulted in the proper matching of the melt viscosity values of PC and PBT/MWCNT. An improvement in the melt viscosity of the matrix polymer in the presence of nanofiller has already been reported by many research groups.[24,25]

Characterizations

Electrical Conductivity. Direct-current electrical conductivity (σ_{dc}) measurements were done on molded specimen bars with dimensions of $30 \times 10 \times 3$ mm^3. The sample was fractured at two ends, and the fractured surface was coated with silver paste to ensure good contact of the sample surface with the electrodes. The electrical conductivities of the conducting nanocomposites were measured with a four-probe method. The specimens were prepared under similar conditions to prevent the influence of the processing parameters on the electrical properties. A minimum of five tests were performed for each specimen, and the data were averaged.

The alternating-current electrical conductivity (σ_{ac}) and dielectric properties of the composites were obtained with a computer-controlled precision impedance analyzer (Agilent 4294A) with the application of an alternating electric field across the sample cell in the frequency range of 40 Hz–10 MHz. The dielectric permittivity (ε') and dielectric loss tangent (tan δ) were obtained as a function of frequency. The σ_{ac} was calculated from the dielectric data with the following relation:

$$\sigma_{ac} \approx \omega \varepsilon_0 \varepsilon' \tan \delta \quad (1)$$

where ω is the angular frequency and is equal to $2\pi f$ (where f is the frequency) and ε_0 is the vacuum permittivity. ε' was determined with the following equation:

$$\varepsilon' \approx C_p / C_0 \quad (2)$$

where C_p is the observed capacitance of the sample (in parallel mode) and C_0 is the capacitance of the cell. The value of C_0 was calculated with the area (A) and thickness (d) of the sample according to the following relation:

$$C_0 \approx (\varepsilon_0 \times A)/d \quad (3)$$

High-Resolution Transmission Electron Microscopy (HR-TEM). The extent of dispersion of the MWCNTs in the PC/PBT matrix phase was studied by HR-TEM (JEM-2100, JEOL, Japan). The PC/PBT–MWCNT nanocomposites were ultramicrotomed under cryogenic conditions with a thickness of around 80–100 nm. The transmission electron microscopy (TEM) images

of the microtomed samples were taken at an accelerating voltage of 200 kV. Because the MWCNTs had a higher electron density, they appeared as black lines in the TEM images.

Field Emission Scanning Electron Microscopy (FESEM). The surface morphology of the PC/PBT–MWCNT nanocomposites was studied with FESEM (Carl Zeiss SUPRA^{TM} 40) with an accelerating voltage of 5 kV. The injection-molded samples were dipped into a liquid nitrogen chamber for 40–50 s, and the samples were fractured under a liquid nitrogen atmosphere. The cryofractured surfaces of the injection-molded samples were gold-coated with a thin layer (approx∼5 nm) to prevent electrical charging. The gold-coated nanocomposite samples were scanned in the vacuum order of 10^{-4} to 10^{-6} mmHg, and SEM images were taken of the fractured surface of the samples.

Differential Scanning Calorimetry (DSC). The glass-transition temperature (T_g) values of the pure PC, PBT, PC/PBT blend, and PC/PBT–MWCNT nanocomposites were determined with DSC (DSC-200 PC, Netzsch, Germany). DSC analysis was done under nonisothermal conditions with 10–12 mg of sample at a scanning rate of 10°C/min under a nitrogen (N_2) atmosphere. First, the samples were heated from room temperature to 230°C, kept for 5 min at that temperature to make the samples moisture free, and then cooled to room temperature at a cooling rate of 10°C/min. Finally, the second heating scans (with the same heating rate and same temperature range) were taken to determine the T_g of the samples.

Dynamic Mechanical Analysis (DMA). The thermomechanical properties of the pure PC, pure PBT, PC/PBT blend, and its nanocomposites were characterized by DMA (DMA 2980 model, TA Instruments, Inc.). The dynamic temperature spectra of the composites were obtained in tension film mode at a constant vibrational frequency of 1 Hz, a temperature range of 30–180°C, and a heating rate of 5°C/min in an N_2 atmosphere. The dimensions of the specimen were $30 \times 6.40 \times 0.42$ mm^3.

Thermogravimetric Analysis (TGA). The thermal stabilities of the pure PC, pure PBT, PC/PBT blend, and PC/PBT–MWCNT nanocomposites were studied with TGA (TGA-209F, Netzsch, temperature accuracy = ±0.5°C). TGA was carried out from room temperature to 700°C in air at a heating rate of 10°C/min. The degradation temperatures of the samples at various stages were calculated from the TGA curves.

RESULTS AND DISCUSSION

Electrical Analysis

σ_{dc}. Figure 2 shows the σ_{dc} values of PC/PBT–MWCNT nanocomposites with different loadings of MWCNTs measured at room temperature. As observed, the σ_{dc} values of the PC/PBT–MWCNT nanocomposites increased with increasing weight percentage of MWCNT loading in the nanocomposites. So, the electrical conductivity of the nanocomposites was directly proportional to the concentration (loading) of the CNTs. With increasing concentration of CNTs in the nanocomposites, an interconnected network path was strongly formed throughout the matrix phase. Finally, by optimizing the PC/PBT–MWCNT nanocomposites, we achieved the electrical conductivity of 6.87×10^{-7} S/cm at an extremely low MWCNT loading (0.35 wt %). This revealed that the continuous conductive network structure of CNT–CNT was formed throughout the PC matrix even at this low concentration of MWCNTs. Thus, the net σ_{dc} of the nanocomposites was greatly improved with increasing concentration of the MWCNTs in the nanocomposites throughout the matrix phase.

Initially, the σ_{dc} values of the PC/PBT–MWCNT nanocomposites with a 0.01 wt % loading of MWCNTs was 1.1×10^{-14} S/cm; this was more or less a similar conductivity value to that of the insulating PC matrix. However, the σ_{dc} values of the PC/PBT–MWCNT nanocomposites greatly increased by several orders ($\sim 10^7$) of magnitude from 10^{-14} to 10^{-7} when the nanocomposites were prepared with a 0.35 wt % loading of MWCNTs. This sudden jump in the conductivity definitely indicated the formation of a continuous conductive interconnected network path of CNT–CNT in the nanocomposites, which is well known as a percolation network. Then, the

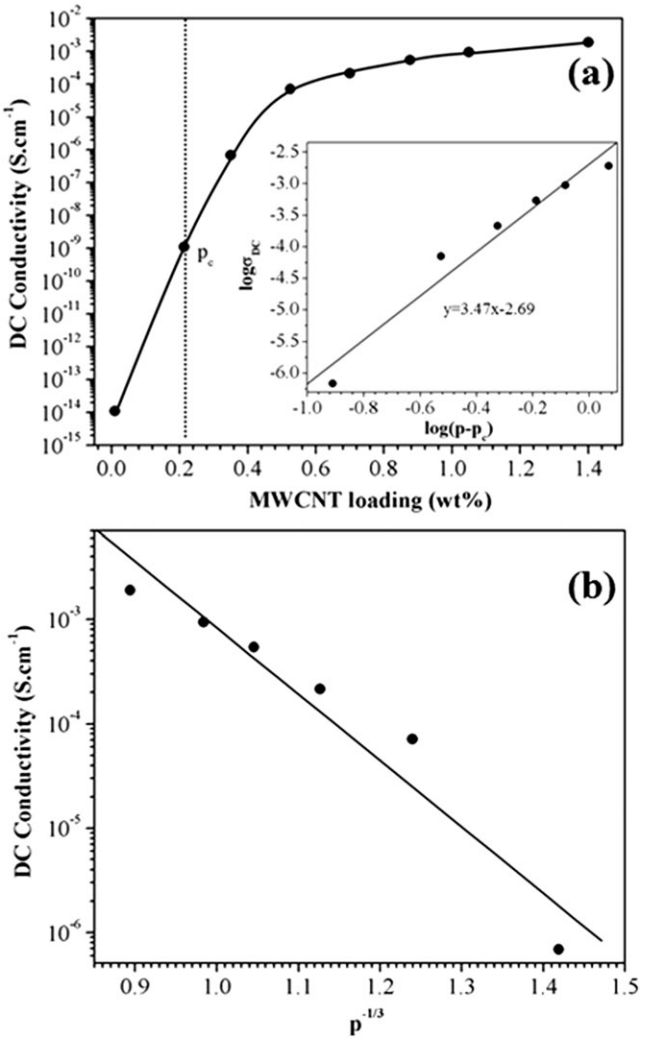

Figure 2. Plot of (a) σ_{dc} versus MWCNT loading and (b) σ_{dc} versus $p^{-1/3}$ for the PC/PBTMWCNT nanocomposites. The inset in figure (a) represents the plot for log σ_{dc} versus log(p − pc) for the same nanocomposites. The straight line in the inset is a least-squares fit to the data with eq. (4) giving the best fit-values (p_c = 0.21 wt % and t = 3.47).

conductivity of the nanocomposites gradually increased with the addition of MWCNTs (from 0.35 to 1.4 wt %) to the PC matrix, and at a 0.7 wt % loading of MWCNTs, the σ_{dc} of the PC/PBT–MWCNT nanocomposites was 2.15×10^{-4} S/cm. This rapid change in the conductivity of the PC/PBT–MWCNT nanocomposites at a 0.7 wt % loading of MWCNTs indicated the unique and homogeneous dispersion of rodlike MWCNTs and the development of a continuous conductive network structure of CNT–CNT throughout the matrix. According to percolation theory, the transition from insulator materials to conductor occurs at a certain concentration (loading) of conducting fillers, known as the *critical concentration*, where the filler particles form a continuous network structure throughout the insulating matrix. The minimum concentration (loading) of the conducting filler at which the nanocomposites show a sudden jump in electrical conductivity is known as p_c.

Many researchers[28,29] have quantitatively predicted the variation of σ_{dc} with different weight percentages (p's) of fillers in conducting polymer nanocomposites on the basis of percolation theory, as shown in Figure 2. Percolation theory has been recognized both theoretically and experimentally. Therefore, σ_{dc} and the static permittivity (ε_s) of polymer nanocomposites near p_c have been studied with power law behavior:

$$\sigma_{dc}(p) = \sigma_0(p - p_c)^t \quad \text{for } p > p_c \tag{4}$$

$$\sigma_{dc}(p) = \sigma_0(p_c - p)^{-s} \quad \text{for } p < p_c \tag{5}$$

$$\varepsilon_s \equiv \varepsilon'(\varphi, f = 0) \propto (p - p_c)^{-s'} \quad \text{for } p < p_c,\ p > p_c \tag{6}$$

where σ_0 is the electrical conductivity of the nanofiller, s' and φ are the critical exponent and volume fraction of the nanofiller, f is the measurement frequency and s and t symbolize critical exponents. The values of the critical exponents strongly vary with the aspect of the percolation system.[8]

The values of the critical exponents t and p_c for the PC/PBT–MWCNT nanocomposites were calculated from the best fitted linear curve of log σ_{dc} versus log$(p - p_c)$ with eq. (4), as shown in the inset of Figure 2(a). The calculated p_c value was about 0.21 wt % for the PC/PBT–MWCNT nanocomposites with a t value of about 3.47. These linear fit values gave an excellent fit with the conductivity of the PC/PBT–MWCNT nanocomposites. This low value of p_c (0.21 wt % loading of MWCNTs) indicated that a continuous conductive CNT–CNT network path was formed throughout the PC matrix and signified a homogeneous dispersion of the high-aspect-ratio, rodlike MWCNTs in the PC/PBT–MWCNT nanocomposites. Thus, σ_{dc} of the nanocomposites was enhanced.

The values of the critical exponent t for two-dimensional (2D) and three-dimensional (3D) lattices have been predicted from various theoretical experiments by many research groups.[30,31] The predicted theoretical t values for the 2D lattice were between 1.10 and 1.43, and it was less than 2.02 for the 3D lattice. The theoretically predicted real part of the conductivity near p_c follows a power law:[24,28]

$$\sigma'(f) \propto f^n \tag{7}$$

At present, the accepted critical exponent (n) values[32] for the equivalent circuit model are about 0.5 and 0.72 in the case of 2D and 3D lattices and about 0.34 and 0.6 for anomalous charge carrier diffusion. According to the equivalent circuit model,[27,28] a random mixture of resistors and capacitors form the percolation clusters. In the case of the charge carrier diffusion model,[32] the diffusion is normal; that is, the charge carriers can travel around different clusters within one period for frequencies $f < f_c$, where f_c is the critical frequency. However, when the frequencies (f) was greater than f_c ($f > f_c$), an anomalous diffusion was observed at the fractal percolation clusters. This is due to the movement of the charge carriers in parts of the percolation cluster within one period. This critical frequency f_c is related with the power law:

$$f_c \propto \frac{1}{\tau_\xi} \propto |\varphi - \varphi_c|^{\nu d_w} \tag{8}$$

where ν stands for the critical exponent related to the cluster size[33] and d_w is the effective fractal dimension of the random walk. The correlation time (τ_ξ) is expressed as the time required by the charge carriers to transverse (explore) a percolation cluster of the correlation length (ξ). Balberg et al.[34] showed that if the nanofillers are considered to be sticks of length L and radius R and p_c is expressed as the fractional volume of the nanofiller (p_c), a relation between the onset of percolation and average excluded volume related to the nanofillers can be written as follows:

$$p_c\left(\frac{L}{R}\right) \approx 3 \tag{9}$$

The conduction in the polymer nanocomposites arises by the tunneling of charge carriers between nanofillers; this depends on the physical contacts among the nanofillers and insulating gaps in their pathways. Thus, the conductive properties of the nanocomposites might change with the effect of the tunneling mechanism.[35] Trujillo et al.[36] reported that the nanofillers might act as a nucleating agent for semicrystalline polymers on the amount of lamellae that may develop around the CNTs.

More recently, the electrical conductivity of different polymer nanocomposites, such as polyepoxy/CNT nanocomposites[37] and polypropylene/CB nanocomposites[38] containing conducting CB and CNTs as nanofillers, has been explained on the basis of a tunneling conduction mechanism. Ryvkina et al.[39] proposed a theoretical model for polymer/CB nanocomposites and explained that the conduction of the nanocomposites was dominated by an electron tunneling mechanism with the following relation:

$$\sigma_{DC} \propto \exp(-Ad) \tag{10}$$

where A is the tunnel parameter and d is the tunnel distance, respectively.

Many researchers have assumed that conducting fillers (CB, CNTs) are randomly or homogeneously distributed in the insulating polymer matrix and that the average distance [tunnel distance (d)] among conducting fillers in the nanocomposites depends on the p value with the relation:

$$d \propto p^{-1/3} \tag{11}$$

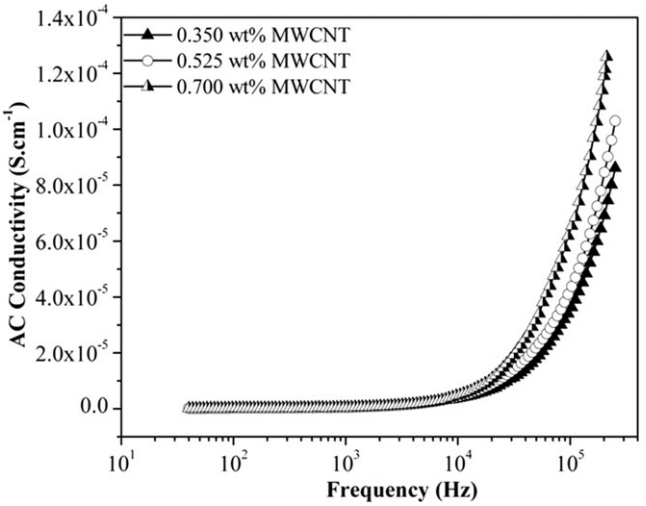

Figure 3. ac conductivity of the PC/PBT–MWCNT nanocomposites versus the frequency at different MWCNT loadings.

It is familiar that the current in a tunnel junction decreases exponentially with the barrier width, which would be, in this case, the mean distance among the nanofillers. Thus, the combination of eqs. (10) and (11) conclude that the value of log σ_{dc} should be directly proportional to $p^{-1/3}$ and can be written as follows:

$$\log(\sigma_{dc}) \propto p^{-1/3} \tag{12}$$

In Figure 2(b), log σ_{dc} for the PC/PBT–MWCNT nanocomposites varied linearly with $p^{-1/3}$; this signified that the tunneling mechanism is one of the main reasons for the electrical conductivity in the nanocomposites. Kilbride et al.[40] reported that individual nanotubes were coated with an insulating polymer; then, the electrical contact between the nanotubes was much less, and contact resistant was very high. When a very skinny layer of polymer existed between the MWCNTs, the tunneling of the electrons occurred between the neighboring CNTs through the polymer. This characteristic of conducting current could be attributed to the tunneling of electrons. In general, the electrons in a polymer cannot move from one electrode to another through the insulator because of the existence of an energy barrier. However, when a voltage is applied between the two, the shape of the energy barrier is changed, and there is a driving force for the electrons to move across the barrier by tunneling; this results in a small current when the distance between neighboring electrodes is sufficiently small so that the electrons in the polymer composites are tunneling one by one from one MWCNT electrode to the nearest MWCNT electrode and forming a CNT–CNT pathway. This reduces the resistance and limits the conductivity of the nanocomposites.

AC Conductivity. Figure 3 shows the variation of the ac electrical conductivity with the frequency in the frequency region of 10^1–10^6 Hz for the PC/PBT–MWCNT nanocomposites measured at room temperature.

As shown in Figure 3, the ac electrical conductivity of the PC/PBT–MWCNT nanocomposites at a constant MWCNT loading increased with increasing frequency. Furthermore, with increasing concentration of MWCNTs, the ac electrical conductivity of the nanocomposites also increased with frequency. This was due to the development of a more continuous conductive network structure throughout the PC matrix with increasing MWCNT loading. In the figure, it is clearly shown that the ac electrical conductivity of the PC/PBT–MWCNT nanocomposites remained almost constant in the frequency region of 50–10^4 Hz, and then, a rapid increase in the conductivity was prominent in the frequency range of 10^4 to 10^6 Hz. The frequency point at which the conductivity rapidly increases with the frequency and beyond which the conductivity strongly depends on frequency is known as f_c.

Several research groups[41,42] have reported that the ac electrical conductivity of the nanocomposites developed because of electron hopping among nanofillers by an electron tunneling mechanism through the layer structures. The conductivity of the nanocomposites is proportional to the rate of electron hopping, and also, electron tunneling occurs over a distribution of conductive pathways. The conductive network path of CNT–CNT in the PC/PBT–MWCNT nanocomposites increased with increasing MWCNT loading, and as a result, the rate of electron hopping or tunneling increased. The aggregate population of electron tunneling pathways had to be above a p_c of the polymer nanocomposites to obtain a significant conductivity.

The frequency dependences of the electrical conductivity of the nanocomposites can be presented by various relations.[43] The response signal to a sinusoidal stimulus was analyzed by Fourier transform by the calculation of the complex impedance, from which the complex dielectric constant $[\varepsilon^*(f)]$ and the complex conductivity $[\sigma^*(f)]$ can be calculated with the following equations:

$$\varepsilon^*(f) = \varepsilon'(f) - i\varepsilon''(f) \tag{13}$$

$$\sigma^*(f) = \sigma'(f) - \sigma''(f) \tag{14}$$

where $\varepsilon'(f)$ and $i\varepsilon''(f)$ denote the real and imaginary parts of the dielectric constant, respectively. On the other hand, $\sigma'(f)$ and $\sigma''(f)$ stand for the real and imaginary parts of the conductivity.

The real part of the conductivity for the nanocomposites, which is a function of the frequency, is calculated through the following relation:

$$\sigma'(f) = 2\pi f \varepsilon_0 \varepsilon''(f) \tag{15}$$

The σ_{ac} of any dielectric material at a low frequency (below f_c) can be expressed in terms of σ_{dc}, ω, and the dielectric loss factor (ε'') with the relation:

$$\sigma_{ac} = \sigma_{dc} + \omega\varepsilon'' \tag{16}$$

The value of σ_{ac} of a dielectric material under frequency is the combination of two components, as shown in eq. (16). The first component represents σ_{dc}; this arises from the ionic or

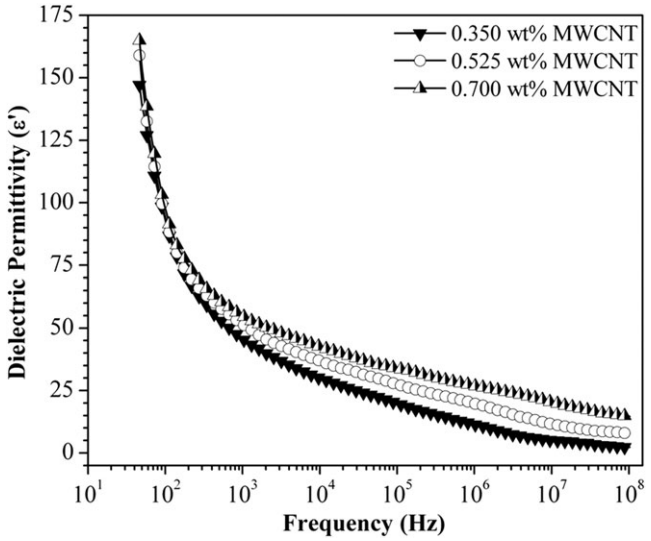

Figure 4. ε' of the PC/PBT–MWCNT nanocomposites versus the frequency at different MWCNT loadings.

electronic conductivity. However, the value of the second component ($\omega\varepsilon''$) in the relation depends on the extent of polarization of dipoles (permanent and induced) and accumulated interfacial charges, which is well known as the Maxwell–Wagner–Sillars effect. At low frequency ($<f_c$), the effect of interfacial polarization becomes more significant as the dipoles/induced dipoles get enough time to orient themselves with the direction of an applied electric field (relaxation phenomena), and thus, the value of σ_{ac} for a conductive system actually represents σ_{dc}. The frequency-independent electrical conductivities up to f_c have already been reported for several disordered materials.[36,40]

At a high frequency ($>f_c$), the polarization effect becomes insignificant as the dipoles get less relaxation time to orient themselves in the direction of the applied electric field. The applied ac electric field (periodic alternation) above f_c results in the radical reduction of space–charge accumulation and the dispersion of dipoles in the applied field direction; this reduces the value of polarization. Thus, the value of σ_{ac} strongly depends on the excitation of the charge particles and the flow of electrons through the continuous conductive network in the matrix phase. Furthermore, it can be assumed that above f_c, the hopping of excited electrons through the interparticle gap (thin polymer layer) becomes easier; this adds to the conductivity that already exists at low frequency in the nanocomposites.

ε'. The variation of the room-temperature ε' of the PC/PBT–MWCNT nanocomposites as a function of the frequency in the frequency region $10^{-}10^{8}$ Hz is shown in Figure 4. These nanocomposites were prepared with various MWCNT loadings in the nanocomposites. As shown in Figure 4, ε' of the nanocomposites rapidly decreased with increasing frequency.

It was observed that in the lower frequency region (50–10^3 Hz), ε' was high and then gradually decreased with increasing frequency. This phenomenon is a well-known behavior of a dielectric material.[44] This type of behavior of dielectric materials could be explained well on the basis of the polarization effect. The ability of the dielectric materials to store energy is attributed to the polarization, that is, electric field-induced separation and alignment of the electric charges; this results in an increase in the capacitance. Accordingly, ε' of a material is proportionally varied with polarizability.[45] In the low-frequency region, the polarization effect is more significant as the molecules of dielectric materials get longer relaxation times to orient them in the direction of the applied electric field and, thus, exhibit a high ε'. With increasing frequency, the relaxation time become insignificant for orientation of the molecules with applied electric field, and the polarization effect becomes unimportant in the dielectric material; this results in a sharp decrease in ε' of the nanocomposites.[46] Thus, after a certain frequency ($\sim 10^4$ Hz) is reached, ε' of the polymer nanocomposites decreases slowly.

As shown in Figure 4, ε' value of the nanocomposites increased with increasing weight percentage of MWCNTs. This improvement in the dielectric properties in the polymer/nanofiller composites could have been due to several factors: (1) the large surface area of nanofillers, which created a large interaction zone or region in the polymer nanocomposites;[47] (2) changes in the polymer morphology due to the surfaces of the fillers; (3) a reduction in the internal field caused by the decrease in the size of the fillers; (4) changes in the space–charge distribution;[48] and (5) a scattering mechanism. Nanofillers have a high surface-area-to-volume ratio, particularly when their size decreases below 100 nm. This high surface-area-to-volume ratio means that for the same particle loading, nanocomposites will have a much higher interfacial area than macrocomposites. In the case of nanofiller-filled materials, the small size of the fillers leads to an exceptionally large interfacial area in the nanocomposites. Because nanofillers have a much higher surface area per unit volume, they possess a much greater interface with their surroundings. The interface controls the degree of interaction between the nanofiller and the polymer matrix and, thus, controls the properties of the nanocomposites. Dissado and Hill[49] reported that the ε' of the nanocomposites started to increase because of the quasi-dc conduction in the low-frequency region. Lewis[50] explained this quasi-dc conduction with the O'Konski's model[51] and a double-layer approach. By this model, charge carriers are efficiently transferred around the interface by the field leading to an induced polarization at the polar ends of the particles.[50] This will lead to a higher dielectric constant. Because these double-layer effects are likely to be pronounced in the nanocomposites, the slope of the permittivity is steeper than that of microcomposites in the low-frequency region.

Morphology Study

Figure 5 represents the electron microscope images of the PC/PBT–MWCNT nanocomposites at a constant MWCNT loading (0.35 wt %). Both PC and PBT polymers are generally immiscible in nature because of their large melt viscosity difference during melt mixing. As shown in Figure 5(a), PC and PBT form an immiscible blend, as indicated by the presence of matrix–droplet morphology in the blend. However, when PC is melt-blended with PBT–MWCNT, these two polymers in the nanocomposites behave like a miscible blend, as shown in the FESEM micrographs of the cross section of the PC/PBT–MWCNT nanocomposites with a 0.35 wt % loading of

Applied Polymer SCIENCE

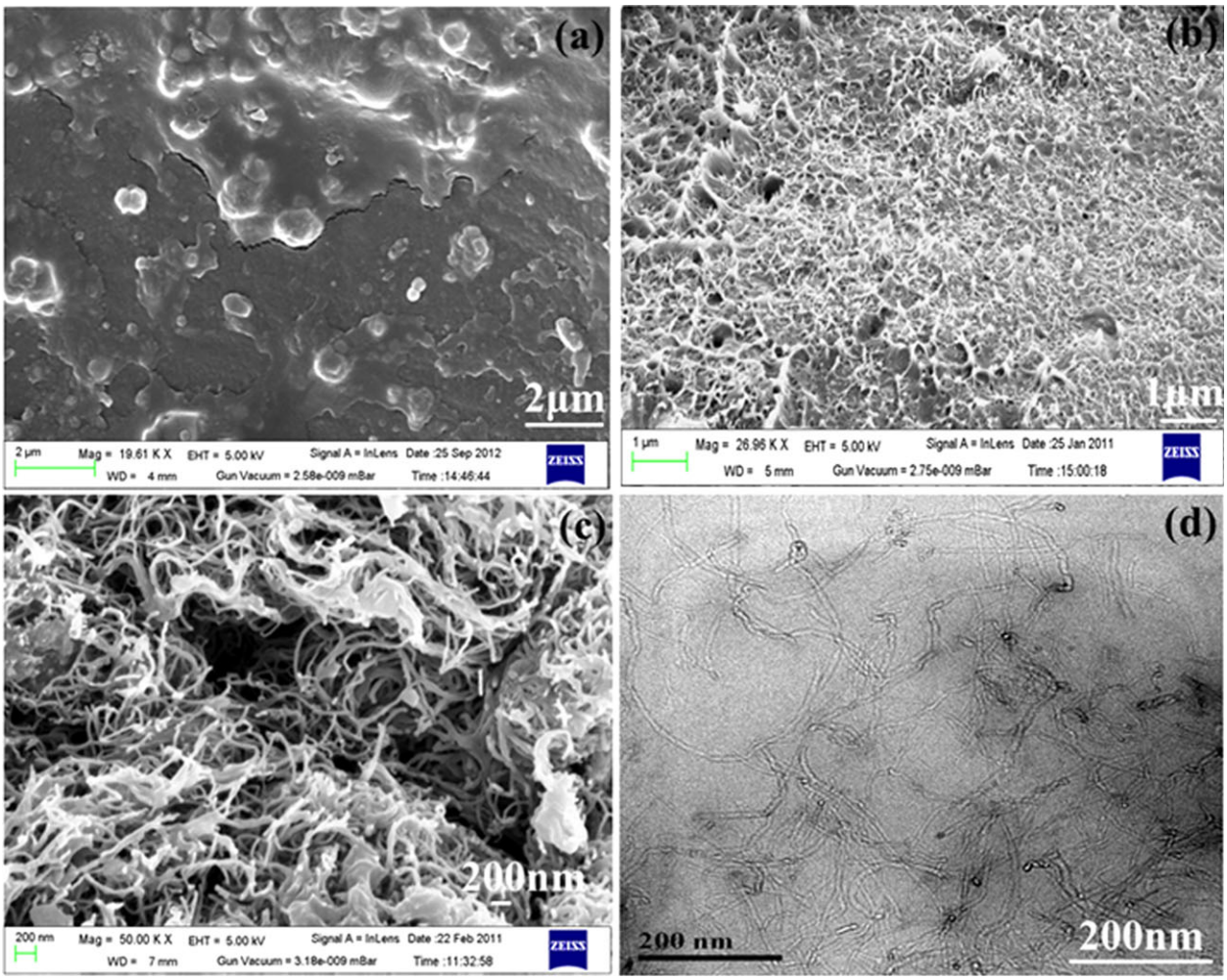

Figure 5. FESEM micrograph of (a) 90 : 10 w/w immiscible PC/PBT blend and (b,c) 90 : 10 w/w PC/PBT–MWCNT nanocomposite at different magnifications and (d) TEM micrographs of the 90 : 10 w/w PC/MWCNT–MWCNT nanocomposites containing 0.35 wt % MWCNTs. [Color figure can be viewed in the online issue, which is available at wileyonlinelibrary.com.]

MWCNTs at different magnifications [Figure 5(b,c)]. As shown in the figure, it was evident that PC and PBT–MWCNT formed a miscible blend in the presence of MWCNTs. Here, the MWCNTs increased the melt viscosity of the PBT and minimized the differences in the melt viscosity of the two polymers. The miscibility behavior of two immiscible polymers in the presence of nanofillers has already been reported by several groups.[52,53] As observed, the MWCNTs were homogeneously distributed throughout the nanocomposites matrix, and an interconnected conductive network path was created in the PC/PBT–MWCNT nanocomposites.

As we observed, the HR-TEM image [Figure 5(d)] clearly indicated the uniform dispersion and distribution of the MWCNTs in the nanocomposites matrix. Moreover, there was no cluster, or selected areas appeared in the nanocomposites for the localization of the CNTs; this demonstrated the formation of a single phase through the miscibility of the PC and PBT–MWCNT phases. This morphology generated a random and continuous electrical-transport path within the insulating PC matrix. Thus, the electrical conductivity properties of the PC changed from an insulating to a semiconducting state with the incorporation of MWCNTs into the insulating polymer matrix. Furthermore, no apparent damage or breakage of the nanotubes was evident in the TEM image; this suggested that melt blending at 280°C and 60 rpm in an internal mixer did not damage the nanotubes.

Thermal Analysis

DSC. Figure 6 shows the second-heating DSC scanning curves of the pure PC, pure PBT, 90 : 10 w/w PC/PBT blend, and 90 : 10 w/w PC/PBT–MWCNT nanocomposites. In the figure, it is shown that the T_g of pure PC was about 147°C and that of pure PBT was about 76°C. In the case of the 90 : 10 w/w PC/PBT blend, a sharp dip along with a small dip in the base line were observed at about 121°C; this signified the T_g of PBT in the blend and the other T_g at about 138°C represented PC in the blend. Thus, the presence of two T_g's and shifting of their values toward each other in the blend indicated the partial miscible nature of the polymers in the blend. However, in the case of the 90 : 10 w/w PC/PBT–MWCNT nanocomposites, a single T_g appeared at about 135°C; this indicated the miscibility of the polymers in the presence of MWCNTs in the nanocomposites.

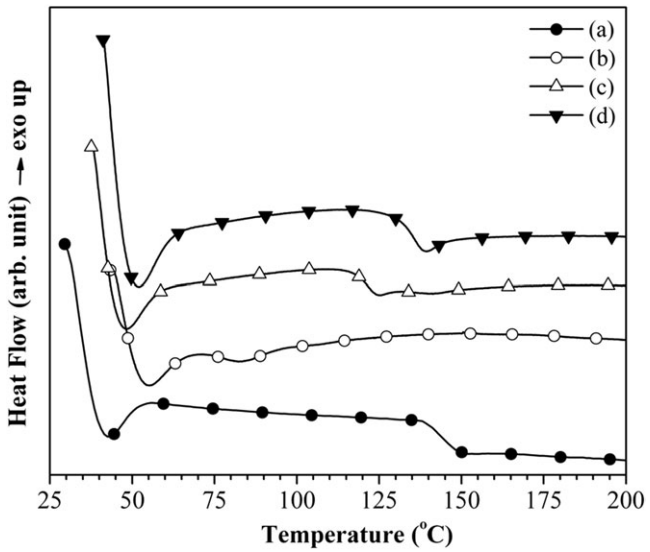

Figure 6. DSC thermograms of the (a) pure PC, (b) pure PBT, (c) 90 : 10 w/w PC/PBT blend, and (d) 90 : 10 w/w PC/PBT–MWCNT nanocomposites with a 0.35 wt % MWCNT loading.

Here, the MWCNTs acted as a viscosity modifier, which increased the melt viscosity of PBT and came close to the melt viscosity of PC and made a miscible blend in the presence of MWCNTs. The incorporation of CNTs in the blend also increased the average T_g of the blend because of the reinforcing effect imparted by the CNTs and polymer–CNT interactions. The interactions between the matrix polymer (PC or PBT) and MWCNTs originated from π–π interactions between the electron-rich phenyl rings of the polymer backbone and the MWCNTs. This interaction retarded the chain mobility of the host polymer and increased the thermal stability of the nanocomposites with the incorporation of the MWCNTs. This kind of interaction between the fillers and polymer in the nanocomposites has already been discussed by different research groups.[54,55]

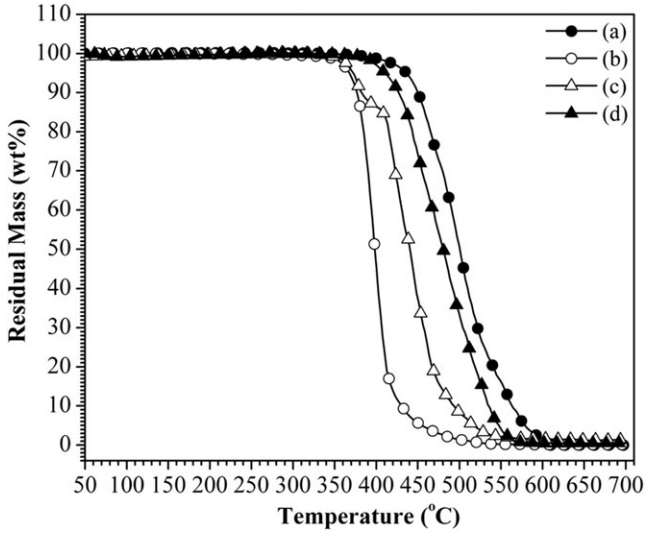

Figure 7. TGA thermograms of the (a) pure PC, (b) pure PBT, (c) 90 : 10 w/w PC/PBT blend, and (d) 90 : 10 w/w PC/PBT–MWCNT nanocomposites with a 0.35 wt % MWCNT loading.

TGA. The TGA thermograms of the pure PC, pure PBT, 90 : 10 w/w PC/PBT blend, and 90 : 10 w/w PC/PBT–MWCNT nanocomposites with a 0.35 wt % MWCNT loading are shown in Figure 7. As observed, the incorporation of MWCNTs into the PC matrix increased the thermal decomposition temperature and the residual yield of the PC/PBT–MWCNT nanocomposites. From the figure, the initial degradation temperature (T_1; the temperature corresponds to a 10% weight loss) and 50% degradation temperature (T_{50}) of the samples were calculated. T_1 of the pure PC began at about 475°C, and T_{50} was observed at about 510°C. T_1 and T_{50} for the pure PBT were calculated at about 380 and 396°C, respectively. The thermal stability of the 90 : 10 w/w PC/PBT blend was lower than that of pure PC, and T_1 of the blend was 385°C. This was due to the incorporation of PBT (which had a lower thermal stability than PC) in the PC matrix. The PC/PBT–MWCNT nanocomposites with a 0.35 wt % loading of MWCNTs was thermally more stable than the PC/PBT blend. T_1 and T_{50} of the PC/PBT–MWCNT nanocomposites were observed at about 425 and 480°C, respectively. The incorporation of the MWCNTs into the nanocomposites formed a shielding barrier against the thermal decomposition of the nanocomposites by acting as the mass- and heat-transfer barriers.[56] Rafailovich et al.[57] reported that CNT layers exhibited a good barrier effect on the thermal degradation products and slowed down the thermal decomposition of the nanocomposites. The CNTs effectively acted as physical barriers to hinder the transport of volatile decomposed products out of the PC/PBT–MWCNT nanocomposites during thermal decomposition. A similar observation was also made in which the CNT layers exhibited a good barrier effect on the thermal degradation process; this led to the retardation of the weight loss rate of the thermal degradation products and to the thermal insulation of polymers in the nanocomposites.[57] Thus, the thermal stability of the nanocomposites was enhanced with the incorporation of a very small quantity of MWCNTs.

DMA. The dynamic mechanical behavior of the pure PC, pure PBT, 90 : 10 w/w PC/PBT blend, and its nanocomposites is shown in Figure 8. As shown in the figure, the thermal stability of the PC/PBT blend improved with the incorporation of a small amount (0.35 wt %) of MWCNTs in the blend–MWCNT nanocomposites. The MWCNTs in the nanocomposites were greatly interconnected with their environment through their greater interface. Thus, the extent of interactions between the nanofillers and matrix polymer in the nanocomposites was significantly controlled by this interface. Sternstein and Zhu[58] studied the viscoelastic behavior of the nanofilled materials and suggested that particulates of nanometric dimensions contributed to the process of tether chain entanglement; this might have had a significant impact on this interaction zone. Because the surface area increased with the incorporation of nanofillers in the nanocomposites, the tethered zones became more important, and the movement of the polymeric chain in the nanocomposites was restricted. This reduction in the chain mobility (in addition to the physical and chemical bonding of the polymer chain with nanofillers) might have contributed to the

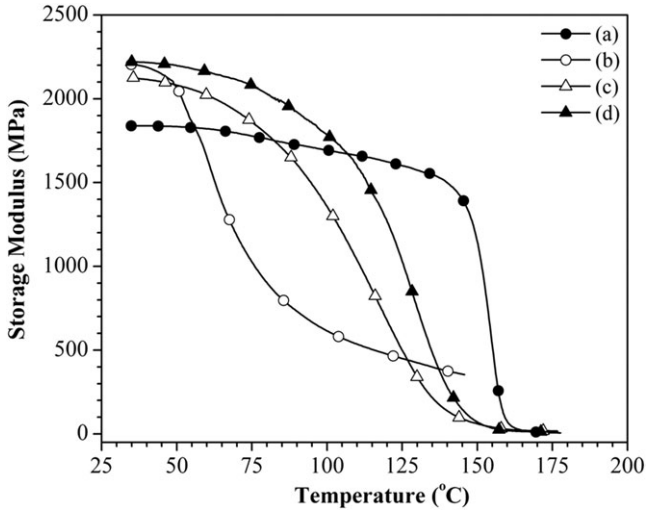

Figure 8. Plot of the storage modulus versus the temperature for (a) pure PC, (b) pure PBT, (c) 90 : 10 w/w PC/PBT blend, and (d) 90 : 10 w/w PC/PBT–MWCNT nanocomposites with a 0.35 wt % MWCNT loading.

reduction in polymer chain relaxation by the formation of crosslinking physical bonds between the polymers and fillers in the nanocomposites. Thus, MWCNTs retarded the chain mobility of the polymers and enhanced the storage modulus of the nanocomposites.

Tan δ. Figure 9 shows the tan δ curve for the pure PC, pure PBT, and 90 : 10 w/w PC/PBT blends without and with MWCNTs. The tan δ peaks of 90 : 10 w/w PC/PBT blend arose at about 138 and 155°C. This value indicated that the PC/PBT blend was immiscible in nature. It is shown that the T_g value of PBT increased, and that of PC decreased after the melt blending of the two polymers. However, only a single tan δ peak was obtained in the case of the PC/PBT–MWCNT (0.35 wt %) nanocomposites at about 154°C. This led us to assume that the

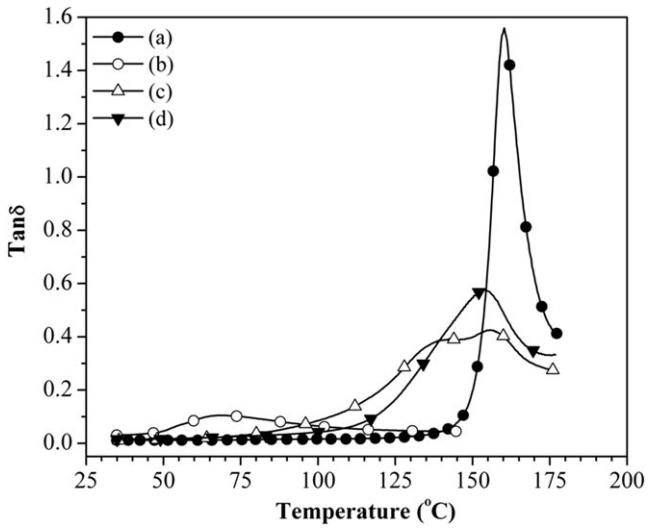

Figure 9. Plot of tan δ versus temperature for the (a) pure PC, (b) pure PBT, (c) 90 : 10 w/w PC/PBT blend, and (d) 90 : 10 w/w PC/PBT–MWCNT nanocomposites with 0.35 wt % MWCNT loading.

PC/PBT blend become compatible with the addition of a small amount of MWCNTs. This suggested that the MWCNTs acted as a viscosity modifier for PBT in the immiscible blend system and formed a miscible blend by controlling the melt viscosity of the two polymers. The incorporation of a small quantity of MWCNTs in the blend increased the T_g value of the nanocomposites compared to the average T_g of the polymer blend without MWCNTs. The MWCNTs retarded the chain segmental motion of the polymers in the nanocomposites and, thus, increased the thermal stability of the nanocomposites.

CONCLUSIONS

In this article, we reported a simple, industrially feasible, straightforward method that involved the melt mixing of PC and a PBT–MWCNT masterbatch to prepare electrically conducting PC/MWCNT nanocomposites at a considerably low loading of unmodified MWCNTs. The miscibility of PBT with PC in the presence of MWCNTs resulted in a homogeneous dispersion of MWCNTs in the PC matrix. Thus, the percolation of MWCNTs in the nanocomposites was shifted to 0.21 wt %; this was significantly lower than previously reported for the PC/MWCNT nanocomposites. ε' of the PC/PBT–MWCNT nanocomposites decreased with increasing frequency; this indicated the possible use of nanocomposites as a dielectric material. The FESEM and TEM studies suggested the homogeneous distribution of MWCNTs in the matrix phase of the nanocomposites. The thermal and mechanical properties of the nanocomposites increased effectively with the incorporation of MWCNTs.

ACKNOWLEDGMENTS

The authors thank the Council of Scientific and Industrial Research, New Delhi, India, for financial support.

REFERENCES

1. Moniruzzaman, M.; Winey, K. I. *Macromolecules* **2006**, *39*, 5194.
2. Li, C. Y.; Li, L.; Cai, W.; Kodjie, S. L.; Tenneti, K. K. *Adv. Mater.* **2005**, *17*, 1198.
3. Chiu, H.-Y.; Hung, P.; Postma, H. W. C.; Bockrath, M. *Nano Lett.* **2008**, *8*, 4342.
4. Gajendran, P.; Saraswathi, R. *J. Phys. Chem. C* **2007**, *111*, 11320.
5. Piper, N. M.; Fu, Y.; Tao, J.; Yang, X.; To, A. C. *Chem. Phys. Lett.* **2011**, *502*, 231.
6. Tang, Y.; Allen, B. L.; Kauffman, D. R.; Star, A. *J. Am. Chem. Soc.* **2009**, *131*, 13200.
7. Yang, R.; Jin, J.; Chen, Y.; Shao, N.; Kang, H.; Xiao, Z.; Tang, Z.; Wu, Y.; Zhu, Z.; Tan, W. *J. Am. Chem. Soc.* **2008**, *130*, 8351.
8. Ci, L.; Suhr, J.; Pushparaj, V.; Zhang, X.; Ajayan, P. M. *Nano Lett.* **2008**, *8*, 2762.
9. LeGrand, D. G.; Bendler, J. T. Handbook of Polycarbonate Science and Technology; Marcel Dekker: New York, **2000**.
10. Wu, T. M.; Lin, Y. W.; Chen, E. C.; Chiang, M. F.; Chang, G. Y. *Polym. Eng. Sci.* **2008**, *48*, 1369.

11. King, J. A.; Michael, D. V.; Jeffrey, A. C.; Mary, M. J.; Ibrahim, M.; Owen, P. M.; Gregg, R. B. *J. Appl. Polym. Sci.* **2010**, *118*, 2512.
12. Hornbostel, B.; Potschke, P.; Koz, J.; Roth, S. *Phys. Status Solidi B* **2006**, *243*, 3445.
13. Jin, S. H.; Choi, D. K.; Lee, D. S. *Colloids Surf. A* **2008**, 313–314, 242.
14. Chen, L.; Pang, X. J.; Yu, Z. L. *Mater. Sci. Eng. A* **2007**, *457*, 287.
15. Yamaguchi, M.; Umishita, K.; Okamoto, K.; Yoon, H. *Polym. Compos.* **2011**, *32*, 97.
16. Kim, K. H.; Jo, W. H. *Carbon* **2009**, *47*, 1126.
17. Abbasi, S.; Carraeau, P. J.; Derdouri, A.; Moan, M. *Rheol. Acta* **2009**, *48*, 943.
18. Potschke, P.; Mahmoud, A. G.; Ingo, A.; Sergej, D.; Dirk, L. *Polymer* **2004**, *45*, 8863.
19. Potschke, P.; Sergej, M. D.; Ingo, A. *Polymer* **2003**, *44*, 5023.
20. Sathpathy, B. K.; Weidisch, R.; Potschke, P.; Janke, A. *Compos. Sci. Technol.* **2007**, *67*, 867.
21. Kim, W. N.; Lee, Y. K.; Han, M. S.; Lee, H. S.; Joo, J. S.; Park, M.; Lee, H. J.; Park, C. R. *Macromol. Res.* **2009**, *17*, 863.
22. Kim, W. N.; Kum, C. K.; Sung, Y.-T.; Han, M. S.; Lee, H. S.; Lee, S.-J.; Joo, J. *Macromol. Res.* **2006**, *14*, 456.
23. Santosa, J. M. R. C. A.; Guthrie, J. T. *J. Mater. Chem.* **2006**, *16*, 237.
24. Kim, J. Y. *J. Appl. Polym. Sci.* **2009**, *112*, 2589.
25. Potschke, P.; Abdel-Goad, M. *J. Non-Newton. Fluid* **2005**, *128*, 2.
26. Singh, B. K.; Kar, P.; Shrivastava, N. K.; Banerjee, S.; Khatua, B. B. *J. Appl. Polym. Sci.* **2012**, *124*, 3165.
27. Zhang, M.; Wu, L.; Wu, D. *J. Polym. Sci. Part B: Polym. Phys.* **2007**, *45*, 2239.
28. Bergman, D. J.; Imry, Y. *Phys. Rev. Lett.* **1977**, *39*, 1222.
29. Stephen, M. *J. Phys. Rev. B* **1978**, *17*, 4444.
30. Fisch, R.; Harris, A. B. *Phys. Rev. B* **1978**, *18*, 416.
31. Gingold, D. B.; Lobb, C. *J. Phys. Rev. B* **1990**, *42*, 8220.
32. Stauffer, D.; Aharony, A. Introduction to Percolation Theory; Taylor & Francis: London, **1994**.
33. Gefen, Y.; Aharony, A.; Alexander, S. *Phys. Rev. Lett.* **1983**, *50*, 77.
34. Balberg, I.; Binenbaum, N.; Wagner, N. *Phys. Rev. Lett.* **1984**, *52*, 1465.
35. Grossiord, N.; Loos, J., van Laake, L.; Maugey, M.; Zakri, C.; Koning, C. E.; Hart, A. *J. Adv. Funct. Mater.* **2008**, *18*, 3226.
36. Trujillo, M.; Arnal, M. L.; Muller, A. J.; Laredo, E.; Bredeau, S.; Bonduel, B.; Dubois, P. *Macromolecules* **2007**, *40*, 6268.
37. Barrau, S.; Demont, P.; Peigney, A.; Laurent, C.; Lacabanne, C. *Macromolecules* **2003**, *36*, 5187.
38. Petrovic, Z. S.; Martinovic, B.; Divjakovic, V.; Budinski-Simendic, J. *J. Appl. Polym. Sci.* **1993**, *49*, 1659.
39. Ryvkina, N.; Tchmutin, I.; Vilcakova, J.; Peliskova, M.; Saha, P. *Synth. Met.* **2005**, *148*, 141.
40. Kilbride, B. E.; Coleman, J. N.; Fraysse, J.; Fournet, P.; Cadek, M.; Drury, A.; Hutzler, S.; Roth, S.; Blau, W. J. *J. Appl. Phys.* **2002**, *92*, 4024.
41. Dickinson, E.; Masui, H.; Williams, M. E.; Murray, R. W. *J. Phys. Chem. B* **1999**, *103*, 11028.
42. Terrill, R. H.; Postlethwaite, T. A.; Chen, C.-H.; Poon, C.-D.; Terzis, A.; Chen, A.; Hutchison, J. E.; Clark, M. R.; Wignall, G.: Londono, J. D.; Superfine, R.; Falvo, M.; Johnson, C. S., Jr.; Samulski, E. T.; Murry, R. W. *J. Am. Chem. Soc.* **1995**, *117*, 12537.
43. Jonscher, A. K. *Nature* **1977**, *267*, 673.
44. Roland, C. M.; Bero, C. A. *Macromolecules* **1996**, *29*, 7521.
45. Shrivastava, N. K.; Khatua, B. B. *Carbon* **2011**, *49*, 4571.
46. Pike, G. E. *Phys. Rev. B* **1972**, *6*, 1572.
47. Ash, B. J.; Siegel, R. W.; Schadler, L. S. *J. Polym. Sci. Part B* **2004**, *42*, 4371.
48. Montanari, G. C.; Fabiani, D.; Palmieri, F.; Kaempfer, D.; Thomann, R.; Mulhaupt, R. *IEEE Trans. Dielectr. Electr. Insul.* **2004**, *11*, 754.
49. Dissado, L. A.; Hill, R. M. *J. Chem. Soc. Faraday Trans. II* **1984**, *80*, 291.
50. Lewis, T. *J. IEEE Trans. Dielectr. Electr. Insul.* **2004**, *11*, 739.
51. O'Konski, C. T. *J. Phys. Chem.* **1960**, *64*, 605.
52. Zaitev, V.; Si, M.; Rafailovich, M.; Chu, B.; Hsiao, B. S.; Liu, L.; Song, H. H.; Gelfer, M. Y. *J. Polym. Sci. Part B: Polym. Phys.* **2003**, *41*, 44.
53. Nazockdast, H.; Dini, M.; Khoshkava, V. *J. Appl. Polym. Sci.* **2012**, *125*, E197.
54. Ye, X.-Y.; Xie, X.-M.; Liu, Y.-T. *Carbon* **2011**, *49*, 3529.
55. Jo, W. H.; Kim, T. K. *Carbon* **2011**, *49*, 819.
56. Orhan, T.; Isitman, N. A.; Hacaloglu, J.; Kaynak, C. *Polym. Degrad. Stab.* **2012**, *97*, 273.
57. Pack, S.; Kashiwagi, T.; Stemp, D.; Koo, J.; Si, M.; Sokolov, J. C.; Rafailovich, M. H. *Macromolecules* **2009**, *42*, 6698.
58. Sternstein, S. S.; Zhu, A.-J. *Macromolecules* **2002**, *35*, 7262.